Tunable White-Light Emission from Conjugated Polymer-Di-Ureasil Materials

ADVANCED FUNCTIONAL MATERIALS

Supporting Information

for *Adv. Funct. Mater.,* DOI: 10.1002/adfm.201504017

Tunable White-Light Emission from Conjugated Polymer-Di-Ureasil Materials

*Niamh Willis-Fox, Mario Kraft, Jochen Arlt, Ullrich Scherf, and Rachel C. Evans**

Supporting Information

Tunable White-Light Emission from Conjugated Polymer-Di-ureasil Hybrid Materials

*Niamh Willis-Fox, Mario Kraft, Jochen Arlt, Ullrich Scherf and Rachel C. Evans**

Email: raevans@tcd.ie

Table of Contents

1. Confocal microscopy

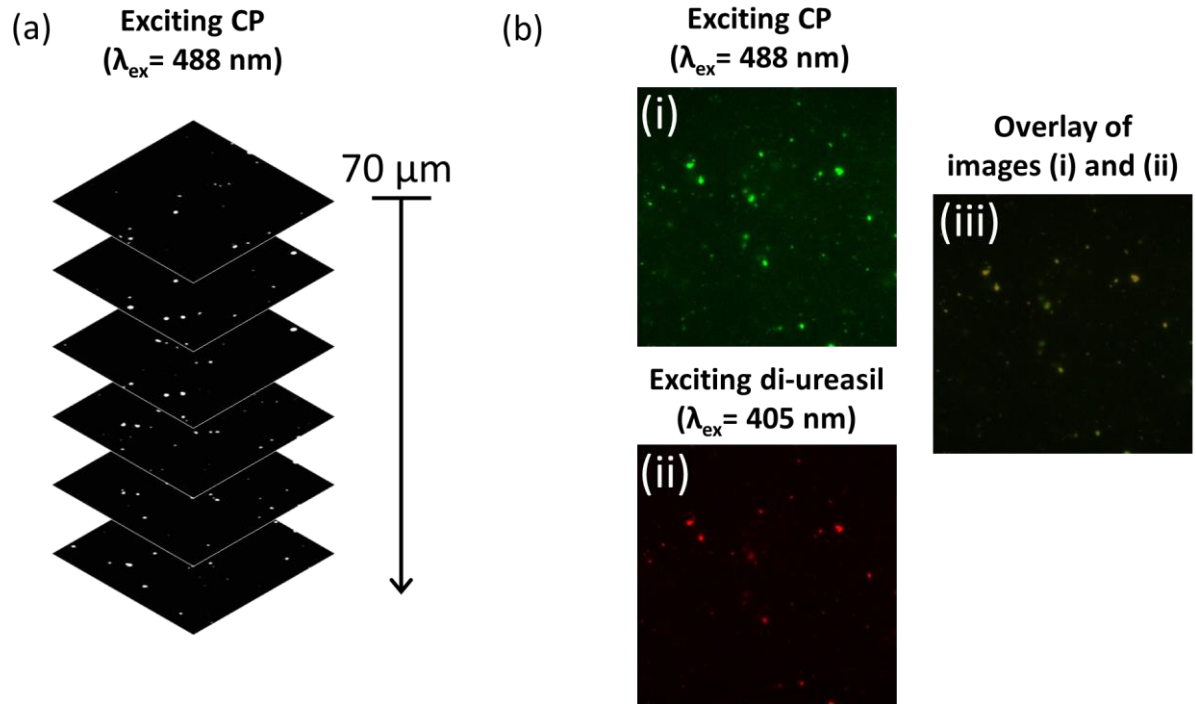

Figure S1. Confocal microscopy images for P3T-6.6 (a) up to a depth of 70 µm from the sample surface (λ_{ex} = 488 nm) and (b) from 40 µm below the surface: (i) λ_{ex} = 488 nm, red emission filter 550-740 nm, (ii) λ_{ex} = 405 nm, red emission filter 550-740 nm and (iii) overlay of images (i) and (ii) showing emission from identical local domains.

2. Powder X-ray diffraction studies

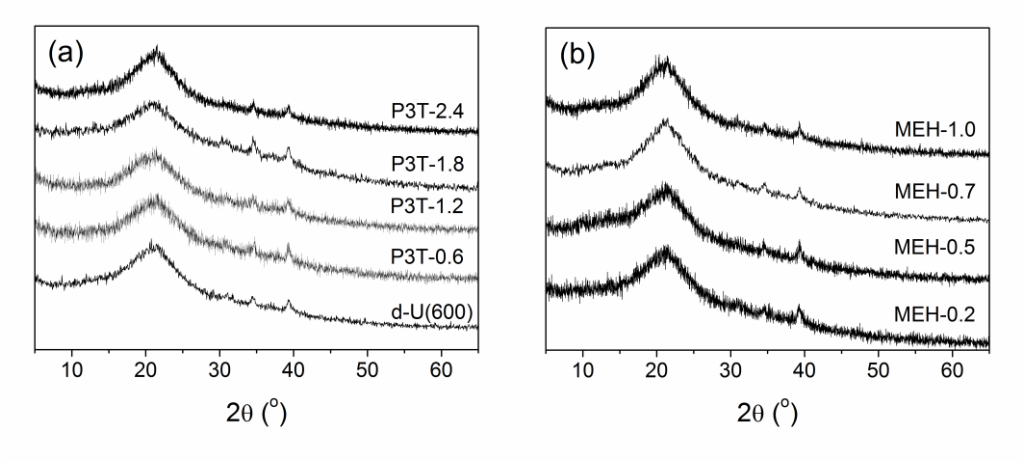

Figure S2. Powder X-ray patterns for samples (a) d-U(600), P3T-0.6, P3T-1.2, P3T-1.8 and P3T-2.4 and (b) MEH-0.2, MEH-0.5, MEH-0.7 and MEH-1.0 in the range 2θ = 5-65°.

3. Solid-state nuclear magnetic resonance (NMR)

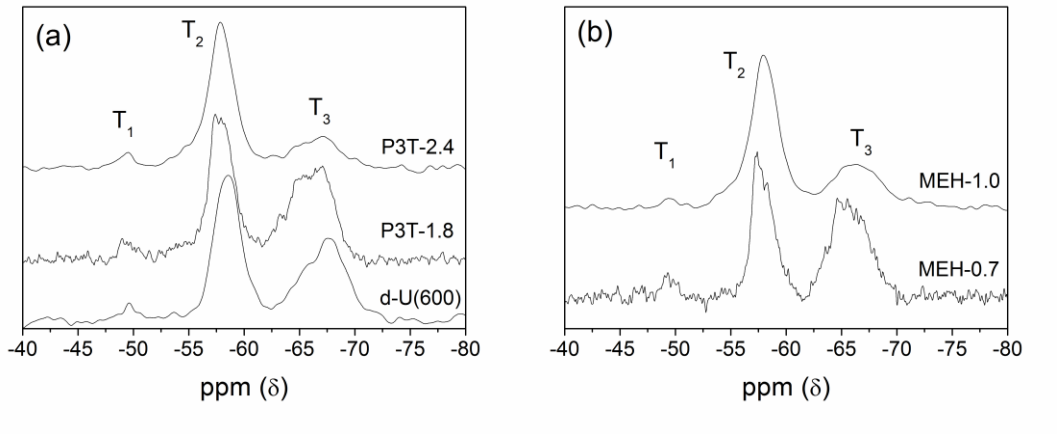

Figure S3. [29]Si solid-state MAS NMR spectra for (a) d-U(600), P3T-1.8 and P3T-2.4 and (b) MEH-0.7 and MEH-1.0.

Table S1: [29]Si MAS NMR chemical shifts (ppm *vs* TMS), population of different T_n species (%), T_n species ratios, and degree of condensation, *C* (%) of CP-di-ureasils.

Sample	T_1 (%)	T_2 (%)	T_3 (%)	T_1:T_2:T_3	C (%)
d-U(600)	-49.7 (3.4)	-58.6 (55.0)	-67.4 (41.6)	1: 16.1:12.2	79.4
P3T-1.8	-49.4 (3.8)	-57.9 (41.3)	-66.8 (54.9)	1: 10.8: 14.4	83.7
P3T-2.4	-49.3 (3.8)	-57.9 (67.0)	-66.9 (29.2)	1: 17.6: 7.7	75.1
MEH-0.7	-49.1 (8.1)	-57.9 (37.6)	-66.9 (54.2	1: 4.6: 6.7	82.0
MEH-1.0	-49.6 (2.6)	-58.0 (62.8)	-66.2 (34.6)	1: 24.2: 13.	77.3

[a] $C = 1/3(\%T_1+2\%T_2+3\%T_3)$[1]

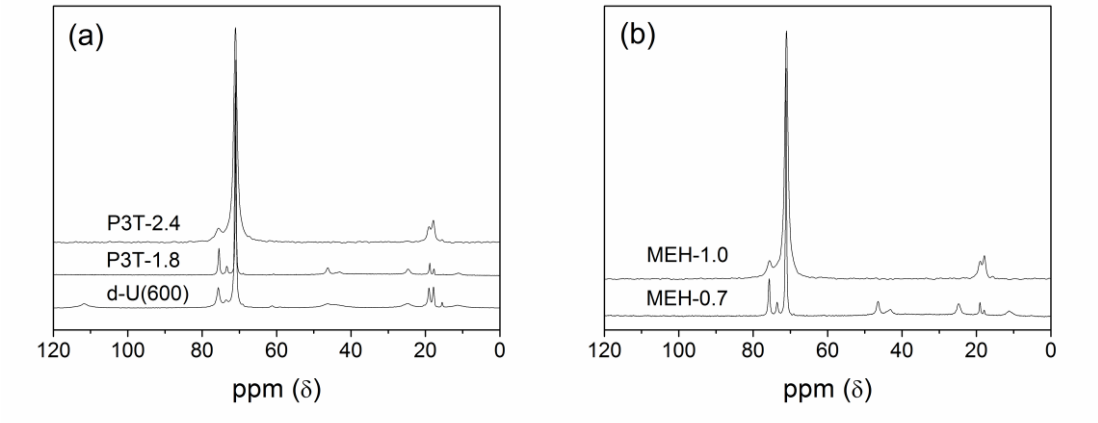

Figure S4. [13]C solid-state CP-MAS NMR spectra for (a) d-U(600), P3T-1.8 and P3T-2.4 and (b) MEH-0.7 and MEH-1.0.

Table S2: ^{13}C solid-state CP-MAS NMR chemical shifts (ppm *vs* TMS) of CP-di-ureasils.

Signal assignment	d-U(600)	P3T-1.8	P3T-2.4	MEH-0.7	MEH-1.0
-OCH	75.7	75.7	75.5	75.7	75.7
-(OCH_2CH_2)	71.1	71.0	71.0	71.2	71.0
-NCH_2 in $N(CH_2)_3Si$	46.3	46.3	-	46.5	-
-'CH_2 in $N(CH_2)_3Si$	24.8	24.6	25.1	24.8	-
-CH_3 in – $OCH_2CH(CH_3)$	19.0	18.8	19.3	19.0	19.0
-CH_3 in – $(CH_3CH_2O)_3Si$	17.8	17.7	17.7	18.0	17.8
-CH_2Si in – $N(CH_2)_3Si$	11.4	11.1	-	11.3	-

4. Fourier transform infrared (FTIR) spectroscopy studies

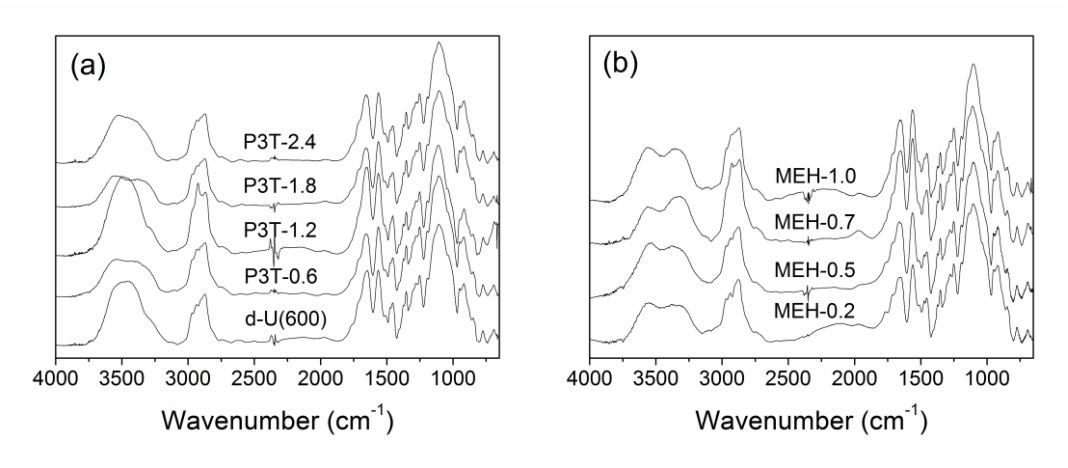

Figure S5. FTIR spectra for (a) d-U(600), P3T-0.6, P3T-1.2, P3T-1.8 and P3T-2.4 and (b) MEH-0.2, MEH-0.5, MEH-0.7 and MEH-1.0 over the range 4000-400 cm^{-1}. Spectra taken at a resolution of 4 cm^{-1}.

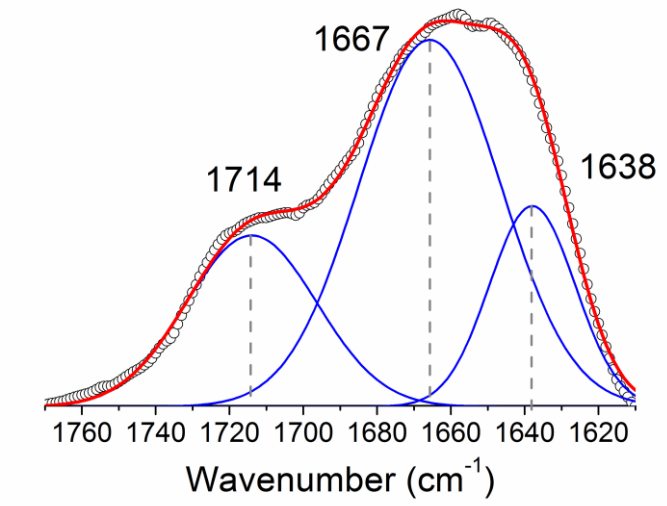

Figure S6. Results of curve-fitting performed in the 'amide I' region of the sample P3T-1.8. The frequencies given are those of the dashed lines and serve solely to guide the eye.

Table S3. Results of the curve fitting performed in the 'amide I' band of MEH-x and P3T-x CP-di-ureasils. The peak position, area and % contribution for each component resolved are shown.

Sample	Peak position	Area (% contribution)	Peak position	Area (% contribution)	Peak position	Area (% contribution)
d-U(600)	1714	0.65 (19.1%)	1665	2.06 (60.4%)	1636	0.70 (20.5%)
P3T-0.6	1713	0.62 (17.8%)	1666	2.16 (61.9%)	1638	0.71 (20.3%)
P3T-1.2	1710	0.41 (12.1%)	1664	2.23 (66.0%)	1637	0.74 (21.9%)
P3T-1.8	1714	0.80 (24.5%)	1666	1.85 (56.7%)	1638	0.61 (18.7%)
P3T-2.4	1714	0.56 (18.8%)	1666	1.86 (62.4%)	1638	0.56 (18.8%)
MEH-0.2	1715	0.39 (21.9%)	1669	1.01 (56.7%)	1639	0.38 (21.3%)
MEH-0.5	1715	0.48 (22.7%)	1668	1.20 (56.9%)	1639	0.43 (20.4%)
MEH-0.7	1714	0.26 (8.4%)	1667	2.09 (67.4%)	1639	0.75 (24.2%)
MEH-1.0	1715	0.69 (21.4%)	1668	1.78 (55.1%)	1639	0.76 (23.5%)

5. Thermogravimetric analysis (TGA)

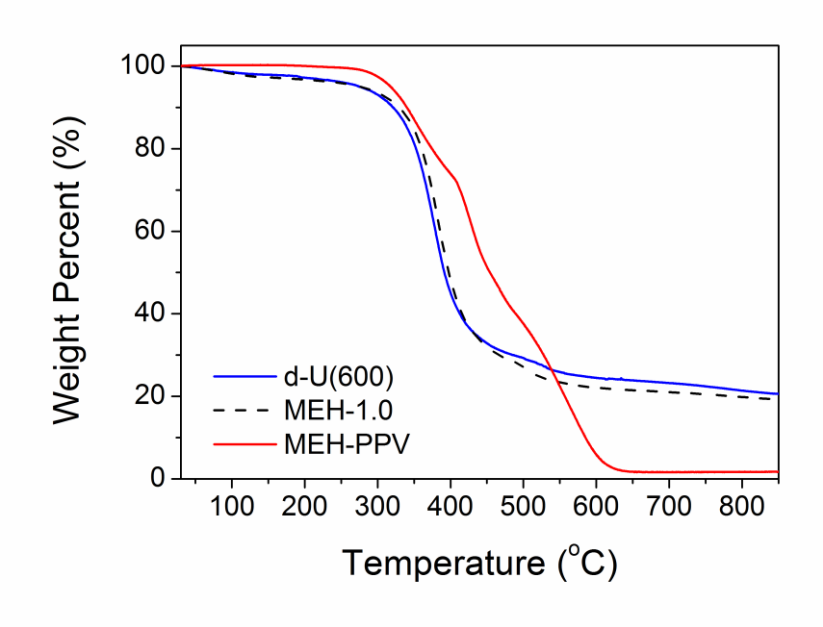

Figure S7. TGA thermograms of d-U(600) (blue solid line), MEH-1.0 (black dashed line) and pure MEH-PPV (red solid line).

Table S4. TGA results showing the onset temperature (T_{os}) and weight loss percentage (%) for CP-di-ureasil samples and the pure CPs.

Sample	T_{os} (˚C) Step One	Weight loss (%)	T_{os} (˚C) Step Two	Weight loss (%)	Sample	T_{os} (˚C) Step One	Weight loss (%)	T_{os} (˚C) Step Two	Weight loss (%)
P3TMAHT	221.8	27.2	435.5	34.6	MEH-PPV	303.7	52.2	508.4	41.3
d-U(600)	334.8	59.4			MEH-0.2	336.1	66.7		
P3T-0.6	336.9	65.8			MEH-0.5	335.2	65.1		
P3T-1.2	337.4	59.7			MEH-0.7	323.8	66.8		
P3T-1.8	337.5	50.6			MEH-1.0	343.9	67.6		
P3T-2.4	328.9	63.8							

6. Photostability study

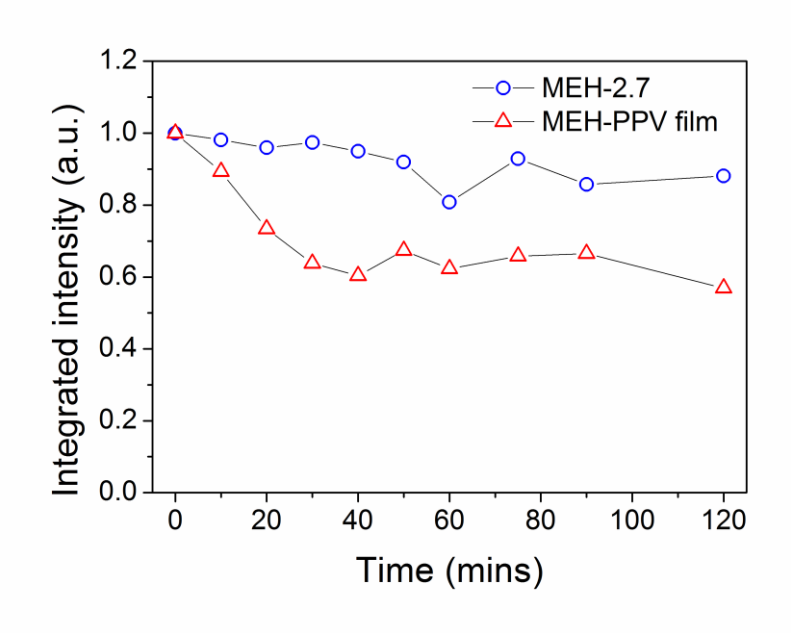

Figure S8. Integrated emission intensity of a MEH-PPV thin film on glass (open red triangles) and MEH-2.7 (open blue circles) under irradiation at 500 nm. The black lines serve only to guide the eye.

7. Steady-state photoluminescence (PL) studies

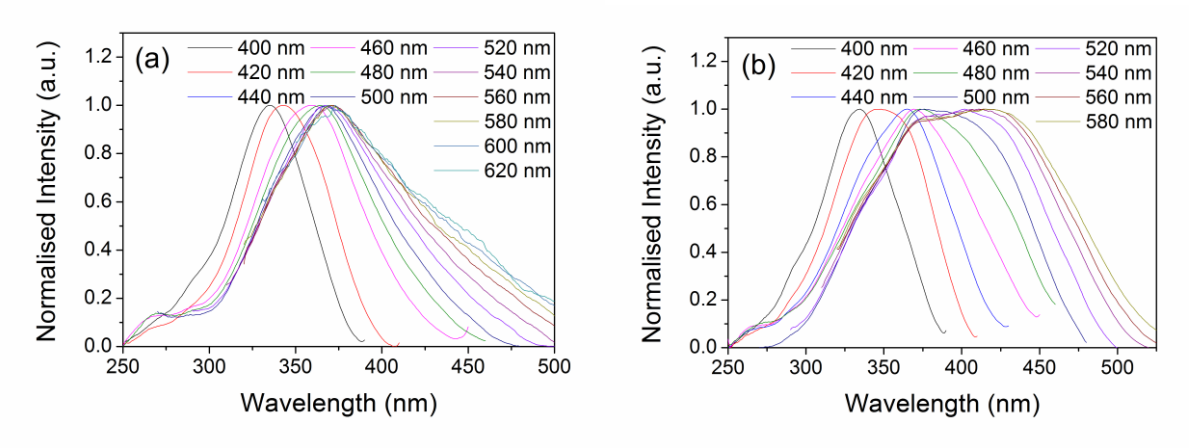

Figure S9. (a) Excitation spectra (λ_{em} = 400, 420, 440, 460, 480, 500, 520, 540, 560, 580, 600 and 620 nm) of d-U(600) and (b) excitation spectra (λ_{em} = 400, 420, 440, 460, 480, 500, 520, 540, 560 and 580 nm) of MEH-0.5.

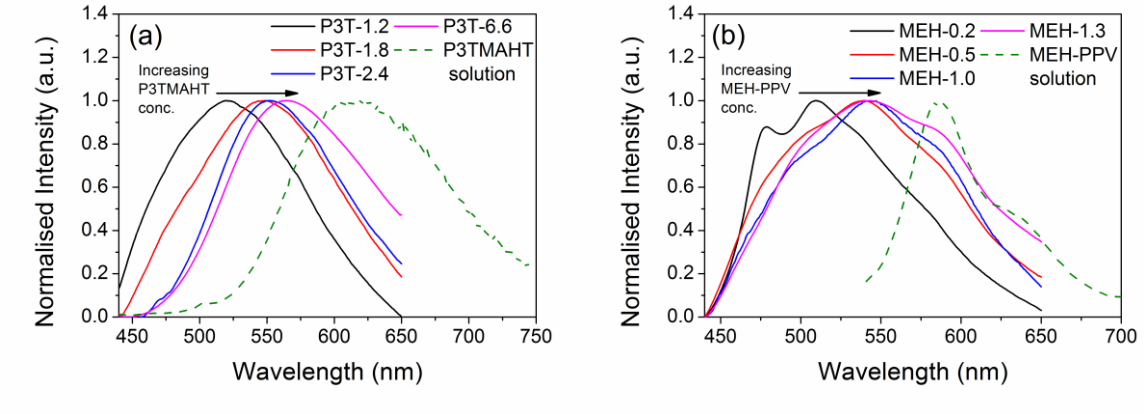

Figure S10. Photoluminescence spectra (λ_{ex} = 430 nm) of (a) P3T-1.2, P3T-1.8, P3T-2.4, P3T-6.6 and P3TMAHT in aqueous solution and (b) MEH-0.2, MEH-0.5, MEH-1.0, MEH-1.3 and MEH-PPV solution (THF).

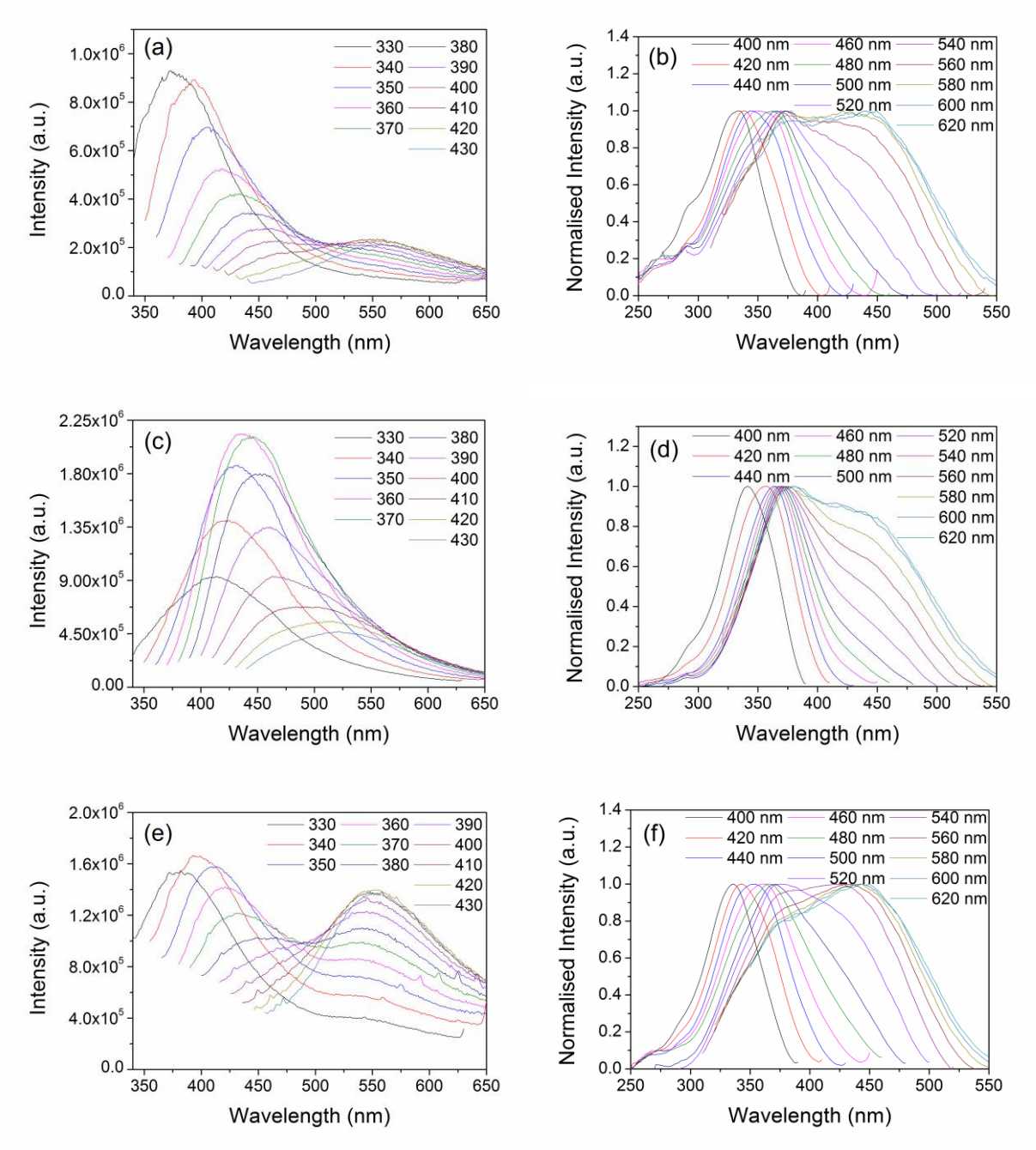

Figure S11. (a) PL and (b) PL excitation spectra of P3T-0.6. (c) PL spectra and (d) PL excitation spectra of P3T-1.2. (e) PL spectra and (f) PL excitation spectra of P3T-2.4. For all PL spectra (λ_{ex} = 330, 340, 350, 360, 370, 380, 390, 400, 410, 420 and 430 nm) and for all PL excitation spectra (λ_{em} = 400, 420, 440, 460, 480, 500, 520, 540, 560, 580, 600 and 620 nm).

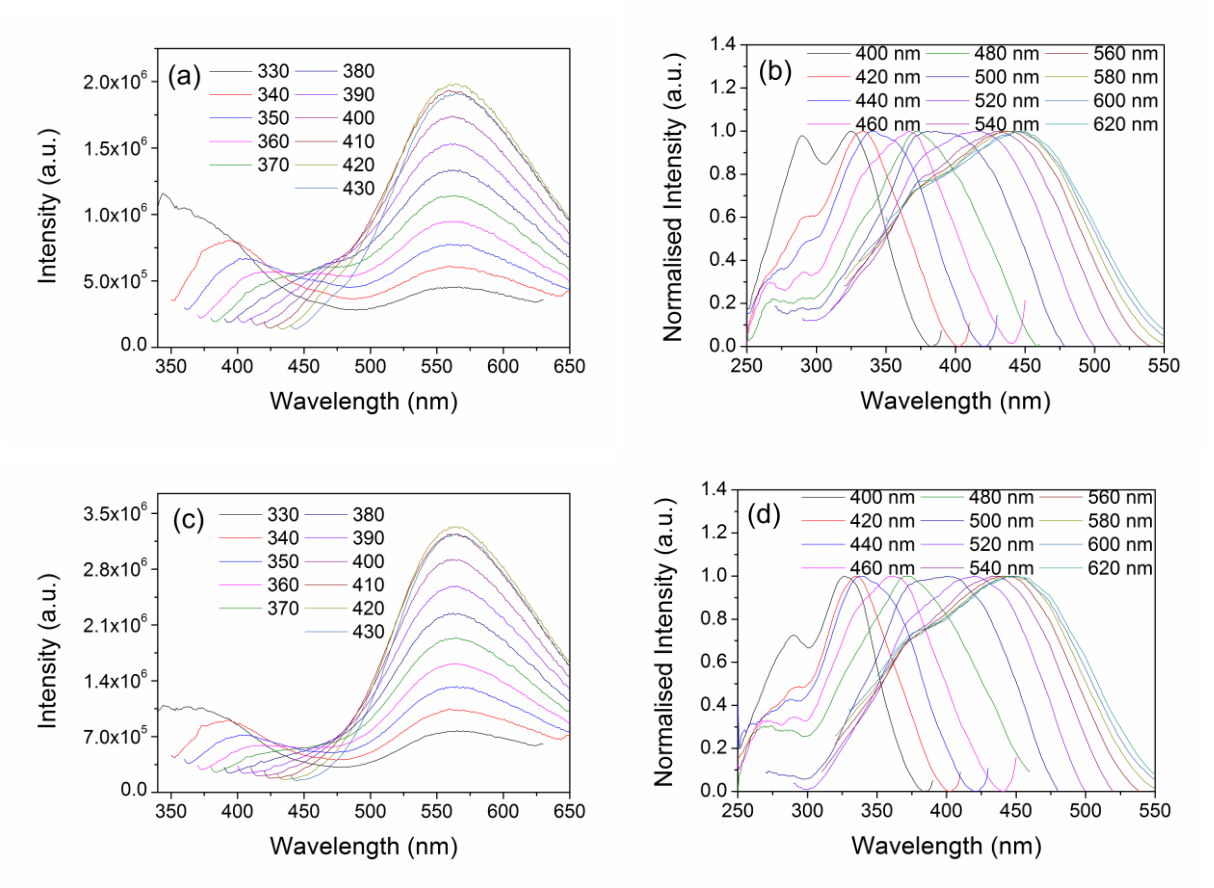

Figure S12. (a) PL and (b) PL excitation spectra of P3T-3.3. (c) PL spectra and (d) PL excitation spectra of P3T-6.6. For all PL spectra (λ_{ex} = 330, 340, 350, 360, 370, 380, 390, 400, 410, 420 and 430 nm) and for all PL excitation spectra (λ_{em} = 400, 420, 440, 460, 480, 500, 520, 540, 560, 580, 600 and 620 nm).

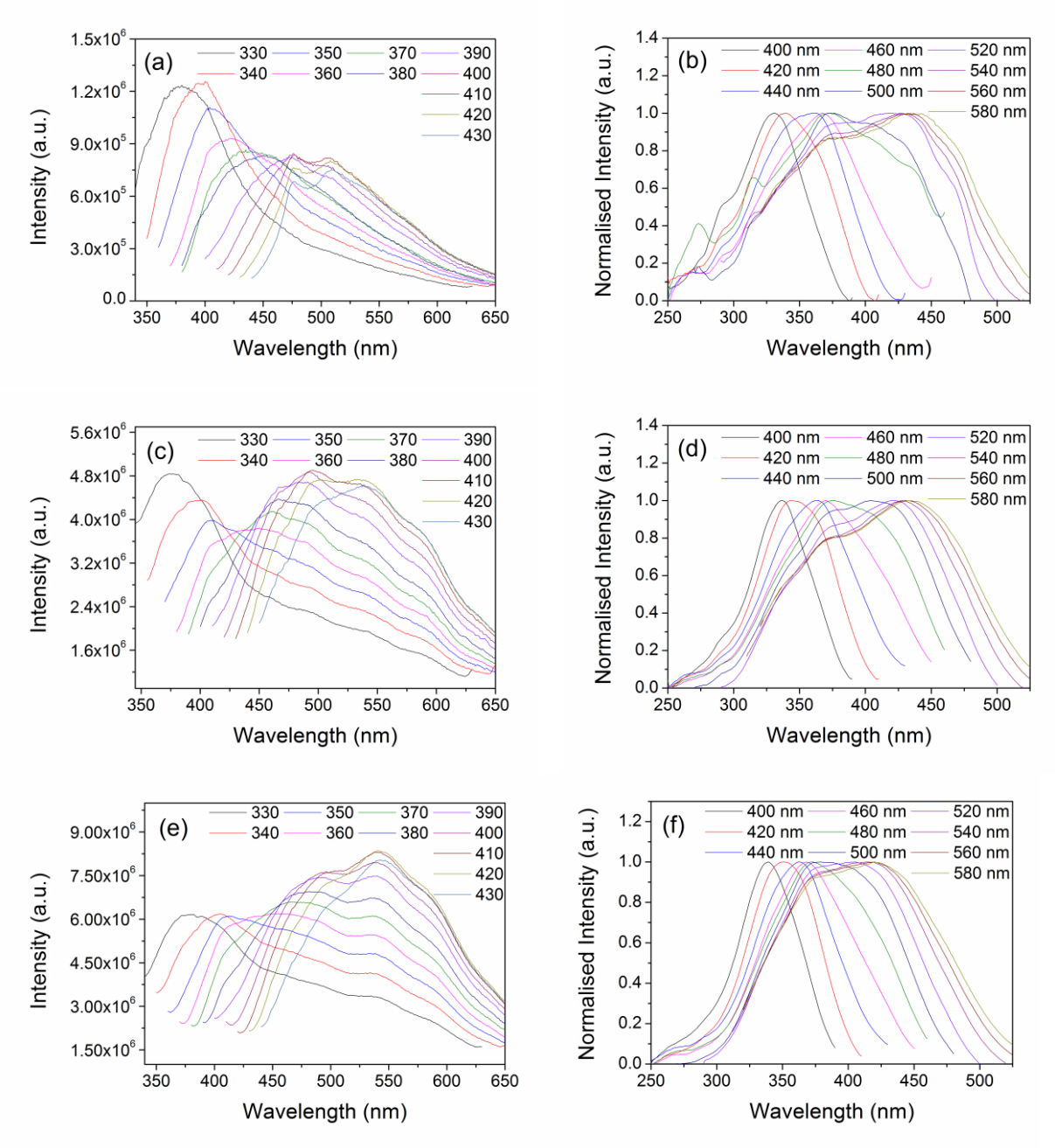

Figure S13. (a) PL and (b) PL excitation spectra of MEH-0.2. (c) PL spectra and (d) PL excitation spectra of MEH-0.7. (e) PL spectra and (f) PL excitation spectra of MEH-1.0. For all PL spectra (λ_{ex} = 330, 340, 350, 360, 370, 380, 390, 400, 410, 420 and 430 nm) and for all PL excitation spectra (λ_{em} = 400, 420, 440, 460, 480, 500, 520, 540, 560 and 580 nm).

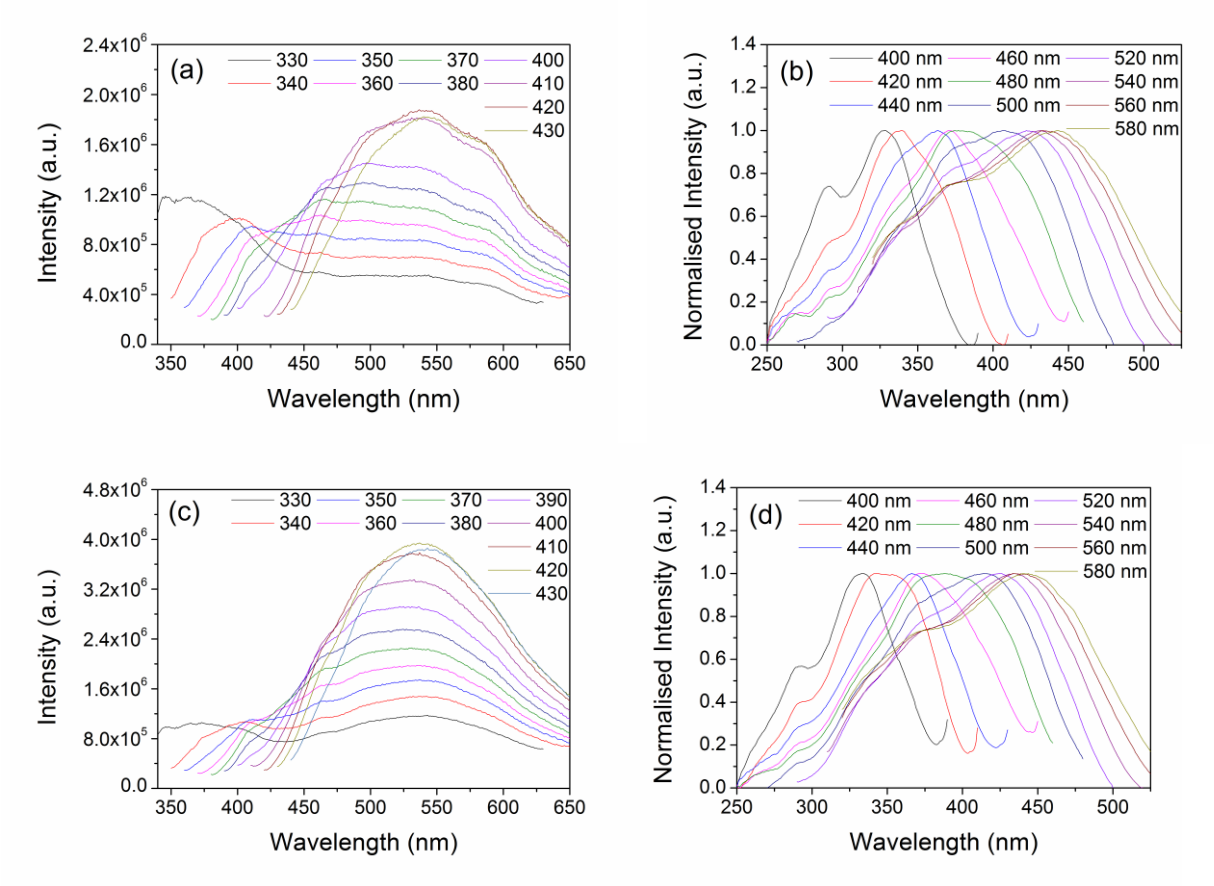

Figure S14. (a) PL and (b) PL excitation spectra of MEH-1.3. (c) PL spectra and (d) PL excitation spectra of MEH-2.7. For all PL spectra (λ_{ex} = 330, 340, 350, 360, 370, 380, 390, 400, 410, 420 and 430 nm) and for all PL excitation spectra (λ_{em} = 400, 420, 440, 460, 480, 500, 520, 540, 560 and 580 nm).

8. Picosecond time-resolved emission decays – data fitting procedure and results

Fluorescence decays were measured for the P3T-x and MEH-x series, upon excitation at 365 nm and detection at 420 and 600 nm, which correspond predominantly to the di-ureasil and CP emission, respectively. All decay curves displayed complex multi-exponential behaviour, requiring a minimum of three exponential components to fit the data. The form of the theoretical multi-exponential decay is given by:

$$I(t) = \sum_i \alpha_i \exp(-t/\tau_i) \quad (1)$$

where α_i and τ_i are the pre-exponential factor and characteristic lifetime for component *i*, respectively. This is the theoretical expression for the response of a sample to an infinitely sharp excitation, also known as a δ-function.[2] In this model, the intensity is assumed to decay as the sum of individual single exponential decays. When examining a single fluorophore displaying a complex decay it is generally safe to assume that the fluorophore has the same radiative decay rate in each environment. Thus, in this case α_i represents the fraction of molecules in each environment at $t = 0$.[3]

The fractional contribution f_i of each decay component to the steady-state intensity can be calculated from:

$$f_i = \frac{\alpha_i \tau_i}{\sum \alpha_i \tau_i} \quad (2)$$

where $\alpha_i \tau_i$ is the area under the decay curve for each decay component.

In reality the excitation pulse is not an infinitely short δ-function and thus the sample does not only decay starting directly after the pulse. Thus, the theoretical sample decay (1) must be reconvoluted with the instrumental response function (IRF) (which includes the width of the excitation pulse and possible electronic responses of the instrument) in the form (3):

$$I'(t) = \int_0^t E(t')I(t-t')dt' \quad (3)$$

where *E(t)* is the excitation pulse and *I(t)* is the theoretical decay model (1). This expression states that the experimentally measured intensity at time *t* is given by the sum of the intensities expected for all δ-function excitation pulses that occur until time *t*, if the excitation pulse is imagined to be comprised as a series of δ-functions with different amplitudes.[4] This model is then fit to the measured decay through the method of non-linear least squares analysis. This is achieved by varying α_i and τ_i until χ^2 is at a minimum. χ^2 is the goodness-of-fit parameter and is described by:

$$\chi^2 = \sum_{i=1}^{n} \left[\frac{y_i - f_{ic}}{y_i^2} \right]^2 \quad (4)$$

where y_i is the measured data, n is the number of data points and f_{ic} is the calculated fit. As α_i and τ_i are varied according to the χ^2 of the previous fit, this method is known as iterative reconvolution. The quality of the non-linear least squares analysis was also judged based on the randomness of the residuals plot. Residuals are the vertical deviation of the measured data points from the fitted curve. Non-random behaviour in the residuals plot suggests a poor fit or a hidden variable.

In some instances it was not possible to obtain satisfactory fits to the data at short times after the pulse (<90 ps). This arises due to the nature of the samples themselves, which makes it impossible to completely eliminate contributions from scattering at the shortest timescales. For these samples, tail fits to the decay curves were used instead.

Tail fits are also carried out using non-linear least squares analysis to reduce the value of χ^2. The difference when compared to the iterative reconvolution method is that for tail fitting the sample curve is not convoluted with the IRF prior to fitting. Tail fitting is only applicable in the region where there is no further sample excitation, *i.e.* only after the excitation pulse has disappeared (e.g. see Fig.S15). While the IRF is needed to choose the correct start channel for the fit, it is not directly required during fitting.

The quality of each of the fits was judged on the basis of the reduced chi-square statistic, χ^2, and the randomness of residuals obtained.

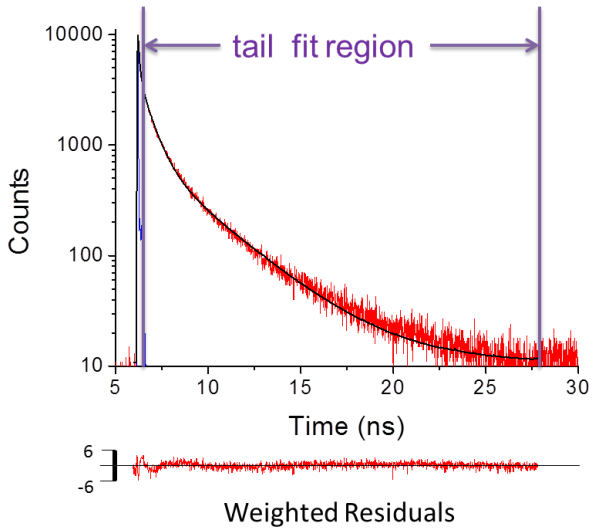

Figure S15. PL emission decay curves (solid red line) (λ_{ex}= 365 nm and λ_{em}= 420 nm), and fit (solid black lines) for P3T-6.6 showing the tail fit region as a representative example. The instrument response function (solid blue line) is also shown.

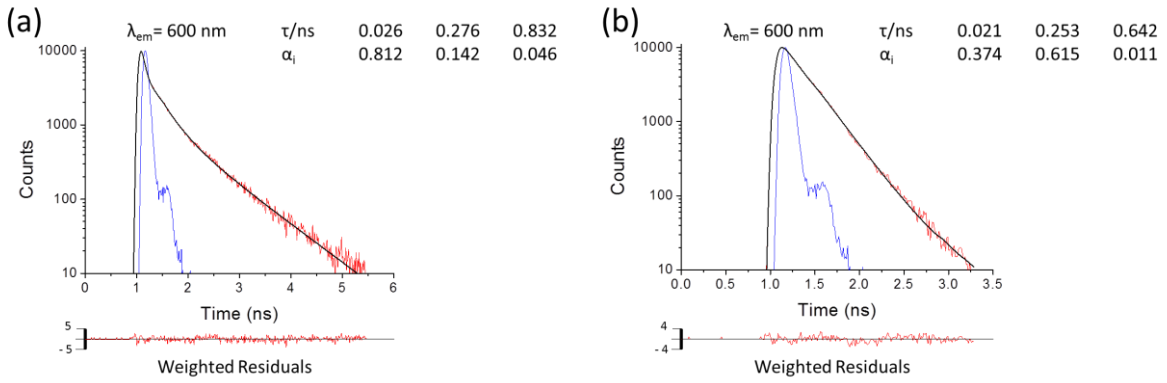

Figure S16. PL emission decay curves (solid red lines) (λ_{ex}= 460 nm and λ_{em}= 600 nm), and fits (solid black lines) for (a) P3TMAHT in water and (b) MEH-PPV in THF. The fitted decay times (τ_i), pre-exponential factors (α_i), fits, weighted residuals and instrument response function (solid blue line) are also shown.

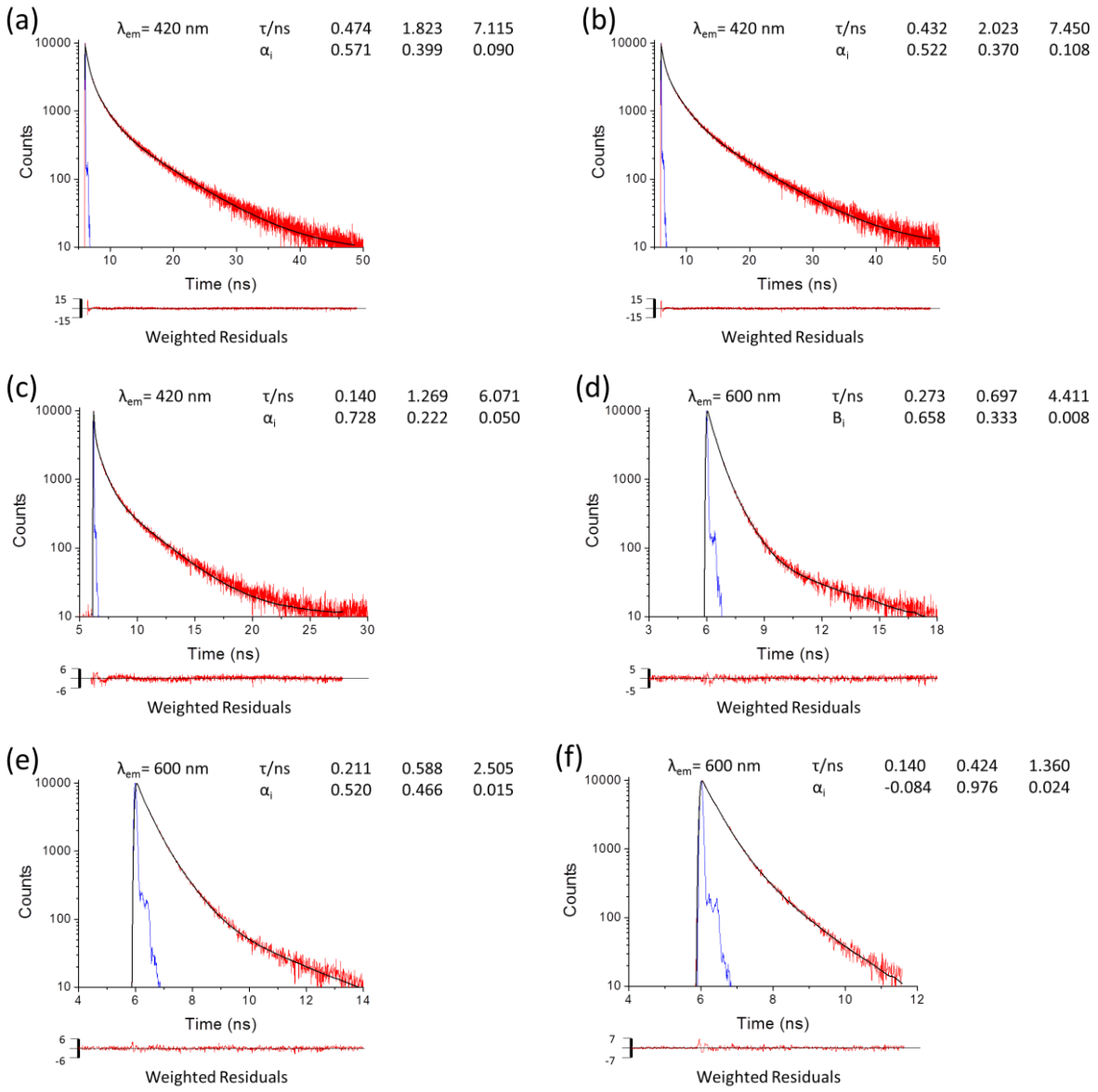

Figure S17. PL emission decay curves (solid red lines), λ_{ex}= 365 nm, and fits (solid black lines) for (a) P3T-1.8 (λ_{em}= 420 nm), (b) P3T-3.3 (λ_{em}= 420 nm) (c) P3T-6.6 (λ_{em}= 420 nm), (d) P3T-1.8 (λ_{em}= 600 nm), (e) P3T-3.3 (λ_{em}=600 nm) and (f) P3T-6.6 (λ_{em}= 600 nm). The fitted decay times (τ_i), pre-exponential factors (α_i), fits, weighted residuals and instrument response function (solid blue line) are also shown.

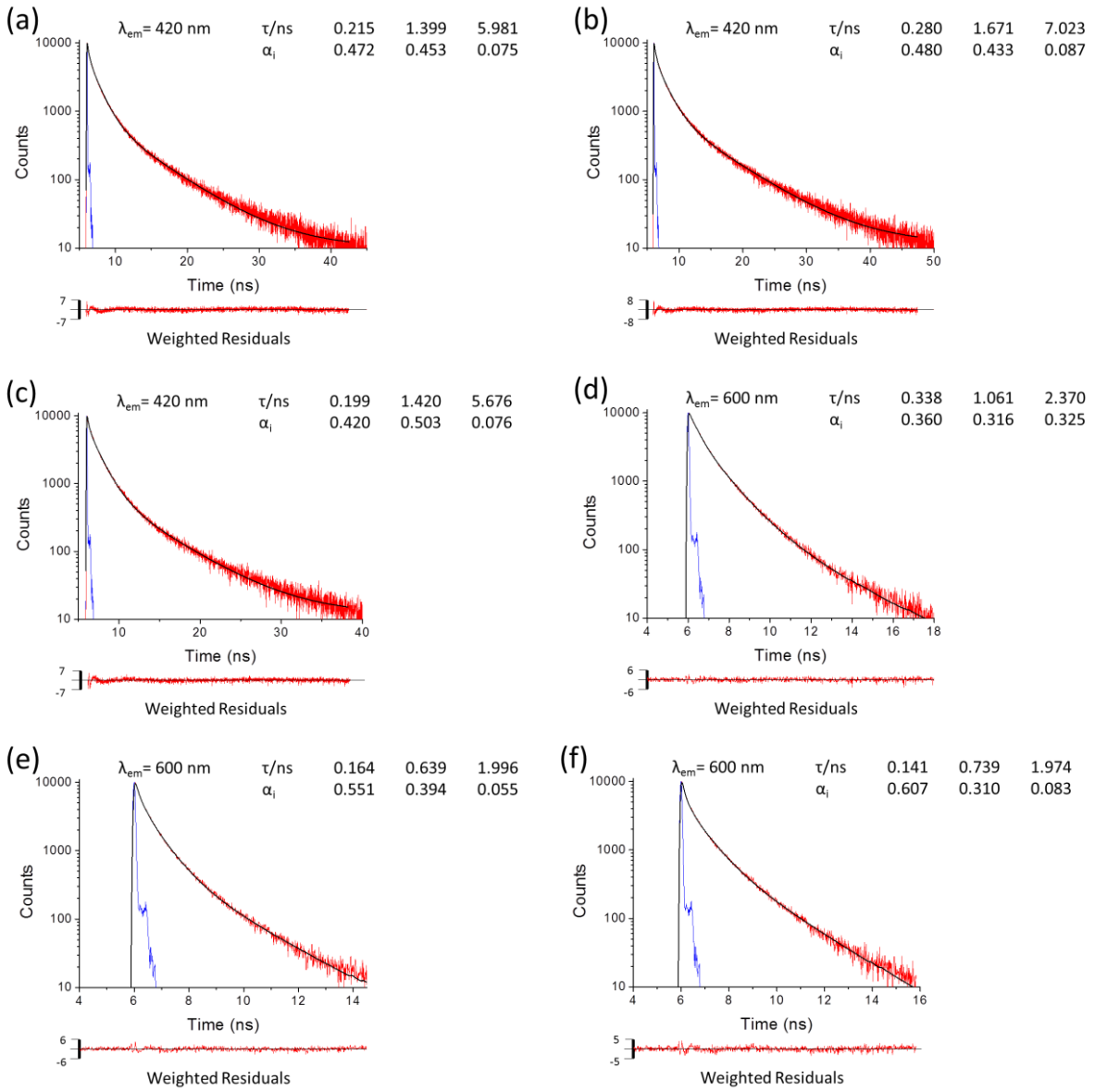

Figure S18. PL emission decay curves (solid red lines), λ_{ex}= 365 nm, and fits (solid black lines) for (a) MEH-0.7 (λ_{em}= 420 nm), (b) MEH-1.3 (λ_{em}= 420 nm) (c) MEH-2.7 (λ_{em}= 420 nm), (d) MEH-0.7 (λ_{em}= 600 nm), (e) MEH-1.3 (λ_{em}=600 nm) and (f) MEH-2.7 (λ_{em}= 600 nm). The fitted decay times (τ_i), pre-exponential factors (α_i), fits, weighted residuals and instrument response function (solid blue line) are also shown.

Table S5. Decay times (τ_i), pre-exponential coefficients (α_i), fractional contribution (f_i) and chi squared (χ^2) values obtained from fitting of the photoluminescence decays (λ_{ex}= 365 nm) of P3T-*x* at λ_{em} = 420 nm.

Sample	τ_1 (ns)	τ_2 (ns)	τ_3 (ns)	α_1	α_2	α_3	f_1	f_2	f_3	χ^2
d-U(600)	0.453 ±0.007	2.459 ±0.022	9.890 ±0.069	0.744 ±0.014	0.208 ±0.004	0.047 ±0.001	0.256 ±0.006	0.389 ±0.008	0.356 ±0.007	1.51
P3T-1.8	0.474 ±0.005	1.823 ±0.041	7.115 ±0.039	0.571 ±0.004	0.339 ±0.002	0.090 ±0.002	0.177 ±0.003	0.404 ±0.011	0.419 ±0.009	1.41
P3T-3.3	0.432 ±0.005	2.203 ±0.031	7.450 ±0.039	0.522 ±0.003	0.370 ±0.002	0.108 ±0.001	0.127 ±0.002	0.422 ±0.007	0.451 ±0.006	1.39
P3T-6.6	0.140 ±0.003	1.269 ±0.021	6.701 ±0.040	0.728 ±0.007	0.222 ±0.002	0.050 ±0.003	0.148 ±0.005	0.409 ±0.013	0.443 ±0.026	1.45

Table S6. Decay times (τ_i), pre-exponential coefficients (α_i), fractional contribution (f_i) and chi squared (χ^2) values obtained from fitting of the photoluminescence decays (P3T-*x* λ_{ex}= 365 and P3TMAHT solution λ_{ex}= 460 nm) at λ_{em} = 600 nm.

Sample	τ_1 (ns)	τ_2 (ns)	τ_3 (ns)	τ_4 (ns)	α_1	α_2	α_3	α_4	f_1	f_2	f_3	f_4	χ^2
P3TMAHT solution	0.026 ±0.001	0.276 ±0.005	0.832 ±0.009		0.812 ±0.024	0.142 ±0.004	0.046 ±0.001		0.215 ±0.010	0.399 ±0.013	0.386 ±0.010		1.11
P3T-1.8		0.237 ±0.005	0.697 ±0.008	4.411 ±0.153		0.658 ±0.016	0.333 ±0.007	0.008 ±0.001		0.401 ±0.012	0.518 ±0.013	0.081 ±0.005	1.1
P3T-3.3		0.211 ±0.006	0.588 ±0.005	2.505 ±0.068		0.520 ±0.015	0.466 ±0.009	0.015 ±0.001		0.261 ±0.011	0.652 ±0.014	0.087 ±0.006	0.95
P3T-6.6		0.236 ±0.007	0.473 ±0.005	1.216 ±0.018		0.422 ±0.014	0.596 ±0.010	0.073 ±0.002		0.233 ±0.010	0.560 ±0.013	0.207 ±0.008	0.97

Table S7. Decay times (τ_i), pre-exponential coefficients (α_i), fractional contribution (f_i) and chi squared (χ^2) values obtained from fitting of the photoluminescence decays (λ_{ex}= 365 nm) of MEH-*x* at λ_{em} = 420 nm.

Sample	τ_1 (ns)	τ_2 (ns)	τ_3 (ns)	α_1	α_2	α_3	f_1	f_2	f_3	χ^2
d-U(600)	0.453 ±0.007	2.459 ±0.022	9.890 ±0.069	0.744 ±0.014	0.208 ±0.004	0.047 ±0.001	0.256 ±0.006	0.389 ±0.008	0.356 ±0.007	1.51
MEH-0.7	0.215 ±0.004	1.399 ±0.013	5.981 ±0.029	0.472 ±0.008	0.453 ±0.008	0.075 ±0.006	0.085 ±0.003	0.534 ±0.020	0.381 ±0.034	1.32
MEH-1.3	0.280 ±0.004	1.671 ±0.016	7.023 ±0.032	0.480 ±0.009	0.433 ±0.008	0.087 ±0.007	0.092 ±0.004	0.494 ±0.019	0.415 ±0.035	1.28
MEH-2.7	0.199 ±0.005	1.420 ±0.014	5.676 ±0.033	0.420 ±0.008	0.503 ±0.008	0.076 ±0.006	0.068 ±0.003	0.580 ±0.020	0.352 ±0.031	1.34

Table S8. Decay times (τ_i), pre-exponential coefficients (α_i), fractional contribution (f_i) and chi squared (χ^2) values obtained from fitting of the photoluminescence decays (MEH-*x* λ_{ex}= 365 and MEH-PPVT solution λ_{ex}= 460 nm) at λ_{em} = 600 nm.

Sample	τ_1 (ns)	τ_2 (ns)	τ_3 (ns)	τ_4 (ns)	α_1	α_2	α_3	α_4	f_1	f_2	f_3	f_4	χ^2
MEH-PPV solution	0.021 ±0.002	0.253 ±0.001	0.642 ±0.036		0.374 ±0.028	0.615 ±0.017	0.011 ±0.001		0.046 ±0.006	0.914 ±0.013	0.039 ±0.005		1.07
MEH-0.7		0.273 ±0.008	1.052 ±0.009	3.073 ±0.064		0.542 ±0.016	0.428 ±0.008	0.030 ±0.001		0.214 ±0.009	0.653 ±0.013	0.133 ±0.007	1.14
MEH-1.3		0.177 ±0.005	0.741 ±0.009	2.095 ±0.033		0.640 ±0.019	0.308 ±0.007	0.051 ±0.002		0.252 ±0.010	0.508 ±0.013	0.240 ±0.008	1.22
MEH-2.7		0.165 ±0.005	0.858 ±0.011	2.100 ±0.033		0.651 ±0.021	0.294 ±0.007	0.055 ±0.002		0.226 ±0.010	0.531 ±0.014	0.243 ±0.008	1.22

9. References

[1] P. P. Lima, R. A. S. Ferreira, S. A. Júnior, O. L. Malta, L. D. Carlos, *J. Photochem. Photobiol. A* **2009**, *201*, 214.

[2] J. R. Lakowicz, in *Principles of Fluorescence Spectroscopy*, Springer, **2006**, p. 99.

[3] J. R. Lakowicz, in *Principles of Fluorescence Spectroscopy*, Springer, **2006**, p. 142.

[4] J. R. Lakowicz, in *Principles of Fluorescence Spectroscopy*, Springer, **2006**, p. 106.